Energy Proceedings
Vol 40, 2024
ISSN 2004-2965

Thermal cycle performance optimization and advantage analysis of an adaptive cycle engine in various bypass modes

Man Zhen[1], Xuezhi Dong[1*], Qiao Zhou[2], Xiyang Liu[1],Chunqing Tan[1]

1 Institute for Aero Engine, Tsinghua University, Beijing, 100084, China

2 COMAC Beijing Aircraft Technology Research Institute, Beijing, 100084, China

(*Corresponding Author: dongxuezhi@tsinghua.edu.cn)

ABSTRACT

With the proposal of carbon neutrality goals, the necessity of reducing carbon in the aviation industry has become increasingly prominent. The advanced aero propulsion technology of adaptive cycle engines poses a new challenge to the traditional engine, which has received widespread attention and high expectations from people. Adaptive cycle engines can change the engine's thermal cycle through adjusting variable geometry schedules to improve engine efficiency, reduce fuel consumption, and increase aircraft cruise time under different missions. In this paper, the optimization variables, constraints, and optimization goals are proposed, and the mathematical performance optimization models of the adaptive cycle engine and the mixed flow turbofan engine are established. Compared with the traditional engines, the control laws of each variable geometry modulation are analyzed in terms of performance matching mechanism, and the regulation necessity of all the variable geometries is discussed. The optimal throttling characteristics lines of the adaptive cycle engine in different bypass modes are calculated by the particle swarm optimization method. The advantageous thrust ranges of the adaptive cycle engine in different operating modes are derived, and the design principles of split ratios is given according to the optimization resultsr.

Keywords: adaptive cycle engine, thermal cycle, split ratio, variable geometry, performance optimization, throttling characteristics

NONMENCLATURE

Abbreviations	
ACE	Adaptive cycle engine
Flade	Fan on blade
FVABI	Front variable area bypass ejector
MSV	Mode selector valve
PSO	Particle Swarm Optimization
RVABI	Rear variable area bypass ejector
Symbols	
B_1	First spilt ratio
B_2	Second spilt ratio
B_3	Third spilt ratio
B_t	Overall bypass ratio
F_s	Specific thrust
F_n	Thrust
H	Altitude
m	Mass flow
Ma0	Flight Mach number
sfc	Specific fuel consumption
π	Pressure ratio
θ_{125}	Opening of FVABI
θ_{163}	Opening of RVABI
η_p	Propulsive efficiency
η_t	thermal efficiency
η_{total}	Overall efficiency

1. INTRODUCTION

By way of airplane heart, the aviation turbine engines become a key factor that determines their ability to fly. Adaptive cycle engines (ACEs) can work in high-efficiency operating modes by adjusting variable geometry to extend the flight time of an airplane and reduce environmental impact, especially the emissions of CO2[1]. ACEs are a key technology for future supersonic transport aircraft development. However, the difficulty of designing an ACE is an excellent challenge for the aerospace industry.

ACEs have many variable geometries, such as the fan-on-blade (Flade) and the mode selector valve (MSV). Many configurations of ACEs have been developed

This is a paper for 15th International Conference on Applied Energy (ICAE2023), Dec. 3-7, 2023, Doha, Qatar.

according to the combination of variable geometries[2-6]. An engine has one or two more bypasses than the traditional turbofan engine, and the variable geometries can adjust the bypass mass flows. An ACE can select the superior working mode according to the matching characteristics. This capability of the ACEs allows the engine to meet thrust requirements while still having a large overall efficiency under different missions.

The ACE has multiple bypasses and variable geometries compared with the traditional turbofan engine. Finding ACE optimal performance is a non-linearity optimization problem with a multi-variable and multi-restriction. Many scholars have contributed various theoretical research on the ACE performance optimization problem, and many advancements have been made. Chen et al.[7] proposed a feasible sequential quadratic programming algorithm to design the optimal control law of a variable cycle engine in different operating conditions. Zheng et al.[8] raised a new optimal matching control schedule method to improve propulsive efficiency by moving the component working points close to their optimal matching lines as the optimization objective. Meng et al.[5] adopted a genetic algorithm to optimize the engine performance of a subsonic climb mission. The results showed that mode 13 has greater thrust than other operating modes. The above studies investigate ACE's optimal performance by different global optimization algorithms. Nature-inspired algorithms have better global convergence than gradient optimization algorithms to solve complex and non-linearity optimization problems[9, 10].

In addition, some research has been conducted for optimization algorithm improvement. Hao et al.[11] presented a novel acceleration technique for the global optimization of VCEs. The technique can significantly reduce the model call number and the convergence number. Qian et al.[12] adopted a modified teaching-learning-based optimization algorithm to optimize the steady state performance of a VCE, and the method gave better optimization results than the genetic algorithm. Zhang et al.[13] proposed an improved DE algorithm with modifying mutation operator. The fuel consumption was reduced by 3.53%, and the specific thrust increased by 4.43%.

The above studies use the determined design cycle parameters to study the optimal performance in different bypass modes. The effect of design cycle parameter variations on the off-design performance of the engine is not considered. However, the effect of design cycle parameters on the engine performance is significant at the design and off-design point.

Meanwhile, there are fewer comparative studies on the performance of adaptive cycle engines and conventional mixed flow turbofan engines. Therefore, the performance optimization model of adaptive cycle engines and conventional mixed flow turbofan engines are established in this study, and various engines with different split ratios are considered. The main goals of contribution are ranked, and the study has differences from other studies as follows:

- A multi-variable and multi-restriction mathematical optimization model for adaptive cycle engines and mixed flow turbofan engines has been developed based on the same technology level.
- The trends of propulsive and thermal efficiencies with the optimal throttling characteristic line are evaluated, and the advantageous operating modes in different thrust ranges are given.
- The effect of different design split ratios on the performance of an adaptive cycle engine under design and non-design conditions and the preferred principles for design split ratios are given.

The remainder of this paper is as follows. Section 2 introduces the engine configuration, while Section 3 presents the optimization strategy for the adaptive cycle engine. Section 4 elaborates on the main results and discussion, and the final section concludes this work.

2. ENGINE STRUCTURE AND CALCULATION METHOD

2.1 Configuration

Fig. 1 presents an ACE with a Flade fan stage[14, 15], which is the configuration of the research object investigated in this paper. Unlike the configuration of the mixed flow turbofan engine, the blades of the first fan stage are extended to the third bypass duct to form a single compression stage. The extra components of the ACE include the following: core engine driven fan (CDFS), front variable area bypass ejector (FVABI), rear variable area bypass ejector (RVABI), mode select valve (MSV), and bypass nozzle.

The primary variable geometries include the variable stator vane of the Flade (VSV_{Flade}), variable stator vane of the CDFS (VSV_{CDFS}), variable stator vane of the HPC (VSV_{HPC}), variable stator vane of the LPT (VSV_{LPT}), nozzle throat area (A_8), FVABI, RVABI, and MSV.

The VSV_{Flade} and the MSV control the opening and closing of the third bypass duct and the second bypass duct, respectively. The ACE can work under four different operating modes through the combined adjustment of the VSV_{Flade} and the MSV. The operating modes are shown in table. 1.

Table 1 The operating modes of the ACE

Modes	First bypass	Second bypass	Third bypass
M1	Open	Close	Close
M13	Open	Close	Open
M12	Open	Open	Close
M3	Open	Open	Open

Three following split ratios are defined to acquire an overview of the system mass flow distribution:

$$B_1 = \frac{m_{125}}{m_{25}} \quad (1)$$

$$B_2 = \frac{m_{13}}{m_{24}} \quad (2)$$

$$B_3 = \frac{m_{113}}{m_{21}} \quad (3)$$

$$B_t = \frac{m_{113} + m_{13} + m_{125}}{m_{25}} \quad (4)$$

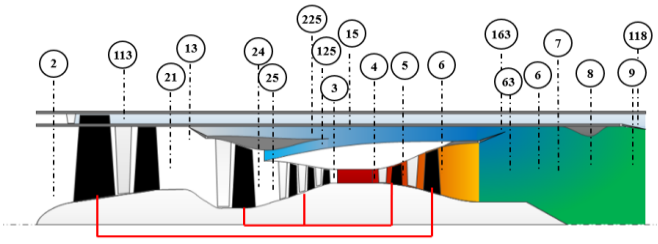

Fig. 1. Configuration and station diagram of the ACE with a Flade fan stage

In order to analyzes the performance enhancement of the adaptive cycle engine compared with the conventional turbofan engine, this section presents several engines with different design parameters. There are three issues that we must pay special attention to in the design point cycle parameters of two types of engines:

1) The turbine forward temperature remains consistent, ensuring that the two types of engines have the same technical level.

2) The inlet corrected mass flow remains consistent, ensuring that the two types of engines have the same inlet size.

3) The fan pressure ratio is determined by keeping the mixer inlet total pressure ratio between 0.95 and 1.05.

The design point of ACE is set at sea-level static condition (H =0 km, Ma0 = 0), and ACE works in mode M3. The design cycle parameters for different engines are shown in Table 2.

Table 2 The design cycle parameters for different engines

Parameter	Turbofan engine		Adaptive cycle engine			
	MI-1	MI-2	AC-1	AC-2	AC-3	AC-4
π_{Flade}	-	-	2.00	2.00	2.00	2.00
π_{Fan}	5.40	4.68	5.15	4.10	4.75	4.85
π_{CDFS}	-	-	1.50	1.50	1.50	1.50
π_{HPC}	5.50	5.50	5.50	5.50	5.50	5.50
T_{t4}	1950	1950	1950	1950	1950	1950
B_1	0.33	0.57	0.10	0.30	0.10	0.10
B_2	-	-	0.10	0.10	0.30	0.10
B_3	-	-	0.10	0.10	0.10	0.30
B_t	0.33	0.57	0.33	0.57	0.57	0.57

2.2 Performance calculation method

There are ten iterative variables to determine the performance of the engine components when the ACE operates in mode M3. There are inhibited by physical conditions, such as the mass flow continuity and power conservation. The iterative variables and balance equations of the ACE are provided in Table 3. Two power balance equations are canceled, and there are eight iteration variables when the ACE works in the transition state. Then, the remaining power drives the rotor to rotate.

Table 3 Iterative variables and balance equations at the design point.

Component	Iterative variable	Balance equations
Flade	β	Mass flow rate
Fan	Bypass ratio and β	
CDFS	Bypass ratio and β	
FVABI		Static pressure
		Mass flow rate
HPC	β	Mass flow rate
HPT	β	Mass flow rate
LPT	β	Mass flow rate
Mixer		Static pressure
Nozzle		Mass flow rate
LP Rotor	N_1	Power
HP Rotor	N_2	Power

The above equations involve nonlinear calculations and interpolation. Hence, the Newton-Raphson method is adopted to obtain the ACE's performance. It possesses good convergence for solving the nonlinear equations of the engines [16-20]. A flowchart of the ACE's off-design performance calculation is exhibited in Fig. 2

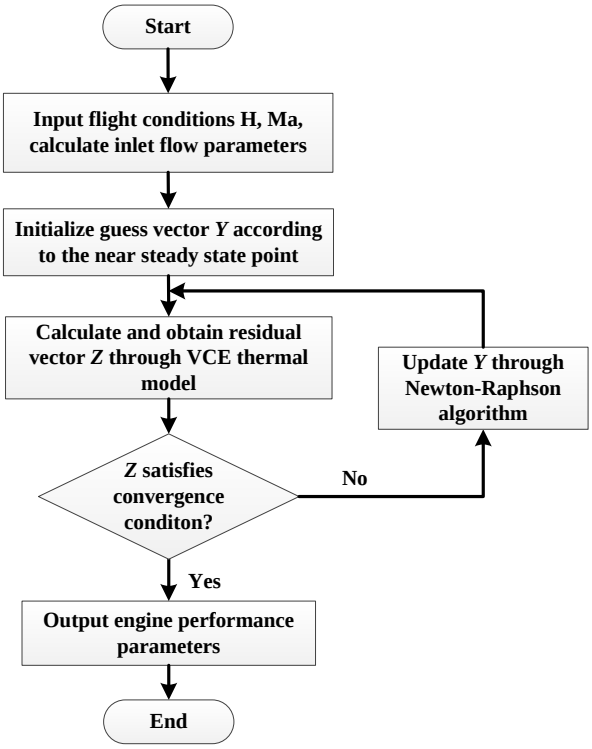

Fig. 2. Flowchart of the ACE's off-design performance calculation

3. OPTIMIZATION ALGORITHMS AND PROCESS

The MSV is not an optimization variable when the ACE works in a specific operating mode. The MSV has only two states: open and closed. According to the setting of the variable geometry, the optimization variables and variation range are shown in Table 4. The opening of β is defined as the ratio of the component openings under different conditions to the design opening area. β_8 and m_f are the optimization variables for mixed flow turbofan engine performance optimization.

Particle Swarm Optimization(PSO) is an evolutionary algorithm-based group collaboration by simulating the behavior of birds foraging developed by Eberhart and Kennedy in 1995[21]. PSO algorithm has been applied widely in many fields[22, 23]. A population contains N numbers of particles, and each particle has its position. The position and velocity of the kth generation of the ith particle can be expressed follows:

$$\boldsymbol{X}_i(\mathrm{k}) = \left(x_{i1}, x_{i2}, \cdots, x_{\mathrm{id}}, \cdots, x_{iD}\right) \tag{5}$$

$$\boldsymbol{V}_i(\mathrm{k}) = \left(v_{i1}, v_{i2}, \cdots, v_{\mathrm{id}}, \cdots, v_{iD}\right) \tag{6}$$

where D is the dimension of the solution space.

The next iteration position is updated based on the current position and velocity. The velocity and the next iteration position are calculated as:

$$\begin{aligned} v_{id}(\mathrm{k+1}) = w \times v_{id}(\mathrm{k}) + c_1 \times r_1 \times \left(p_{id}(\mathrm{k}) - x_{id}(\mathrm{k})\right) \\ + c_2 \times r_2 \times \left(p_{gd}(\mathrm{k}) - x_{id}(\mathrm{k})\right) \end{aligned} \tag{7}$$

$$x_{id}(\mathrm{k+1}) = x_{id}(\mathrm{k}) + v_{id}(\mathrm{k+1}) \tag{8}$$

where w is the inertia weight used to balance the algorithm's local and the global search abilities; c_1 and c_2 are the acceleration coefficients; and r_1 and r_2 are randomly generated numbers in the range [0, 1].

The optimization goals need to determined after selecting the optimal algorithm. According to different flight missions, the optimization goals of engines are generally divided into two categories. The largest thrust optimization goal is calculated when the engine works in high-power conditions, such as maximum Mach number, take-off, spiral trajectory, etc. The optimization variable combination is:

$$\boldsymbol{X} = \left[VSV_{\mathrm{Flade}}, VSV_{\mathrm{CDFS}}, VSV_{\mathrm{HPC}}, VSV_{\mathrm{LPT}}, \beta_{125}, \beta_{163}, \beta_8, m_{\mathrm{f}}\right] \tag{9}$$

The optimization goal is given by:

$$\begin{cases} \max F_{\mathrm{n}}\left(\boldsymbol{X}\right) \\ \text{s.t. } VSV_{\mathrm{Fan}} \in I_1, VSV_{\mathrm{CDFS}} \in I_2, VSV_{\mathrm{HPC}} \in I_3 \\ VSV_{\mathrm{LPT}} \in I_4, \beta_{125} \in I_5, \beta_{163} \in I_6, \beta_8 \in I_7, \mathrm{MSV} \in \{0,1\} \\ \mathrm{SM}_{\mathrm{Flade}} \geqslant 10\%, \mathrm{SM}_{\mathrm{Fan}} \geqslant 10\%, \mathrm{SM}_{\mathrm{CDFS}} \geqslant 10\%, \mathrm{SM}_{\mathrm{HPC}} \geqslant 10\% \\ \mathrm{RM} \geqslant 10\%, N_1, N_2 \leqslant 105\%, T_{\mathrm{t3}} \leqslant T_{\mathrm{t3max}}, T_{\mathrm{t4}} \leqslant T_{\mathrm{t4max}} \end{cases} \tag{10}$$

where I_1, I_2, I_3, I_4, I_5, and I_6 are the feasible ranges of the corresponding optimization variables shown in Table 4.

The other optimization goal is the minimum specific fuel consumption when the engine works in cruising conditions under a specific thrust. The optimization variable combination is:

$$\boldsymbol{X} = \left[VSV_{\mathrm{Flade}}, VSV_{\mathrm{CDFS}}, VSV_{\mathrm{HPC}}, VSV_{\mathrm{LPT}}, \beta_{125}, \beta_{163}, \beta_8\right] \tag{11}$$

The optimization goal is given by:

$$\begin{cases} \min sfc\left(\boldsymbol{X}\right) \\ \text{s.t. } VSV_{\mathrm{Fan}} \in I_1, VSV_{\mathrm{CDFS}} \in I_2, VSV_{\mathrm{HPC}} \in I_3 \\ VSV_{\mathrm{LPT}} \in I_4, \beta_{125} \in I_5, \beta_{163} \in I_6, \beta_8 \in I_7, \mathrm{MSV} \in \{0,1\} \\ \mathrm{SM}_{\mathrm{Flade}} \geqslant 10\%, \mathrm{SM}_{\mathrm{Fan}} \geqslant 10\%, \mathrm{SM}_{\mathrm{CDFS}} \geqslant 10\%, \mathrm{SM}_{\mathrm{HPC}} \geqslant 10\% \\ \mathrm{RM} \geqslant 10\%, N_1, N_2 \leqslant 105\%, T_{\mathrm{t3}} \leqslant T_{\mathrm{t3max}}, T_{\mathrm{t4}} \leqslant T_{\mathrm{t4max}} \\ F_{\mathrm{n}} = \text{constant} \end{cases} \tag{12}$$

Table 4 Variable Geometry initial settings and variation values

Variable geometry	Value range
VSV_{Flade}/°	[-85, 0]
VSV_{CDFS}/°	[0, 45]
VSV_{HPC}/°	[-10, 10]
VSV_{LPT}/°	[-10, 10]
β_{125}	[0.1, 1.0]
β_{163}	[0.1, 1.0]
β_{8}	[0.8, 1.2]

4. SIMULATION RESULTS AND DISCUSSION

4.1 Speed-height characteristic

Fig. 3 illustrates the optimization results of speed altitude characteristics of the different engine configurations using the maximum thrust optimization mode. The maximum thrust of the ACE is higher than the mixed flow turbofan engine with the same overall bypass ratio as shown in Fig. 3 a) and b). The increase of B_1 can enhance the thrust capability at low altitudes and high Ma numbers. The F_n increases significantly with the

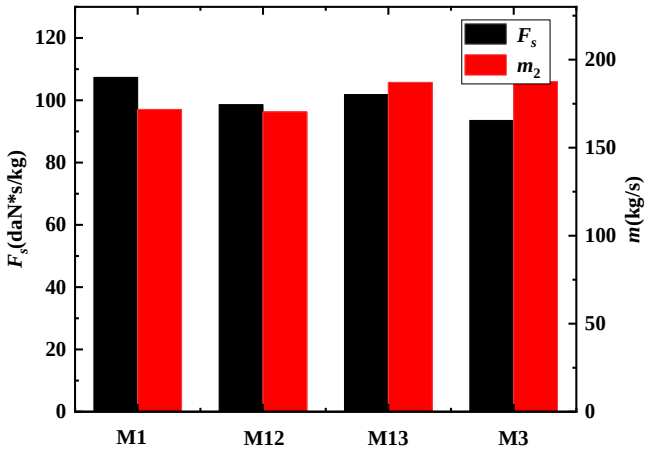

Fig. 4. Optimization results of the inlet mass flow and specific thrust of AC-2

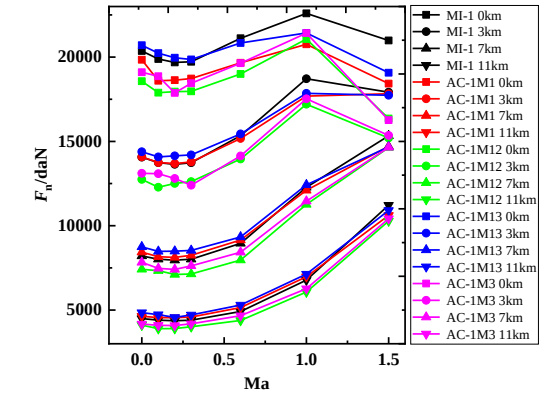

a) AC-1

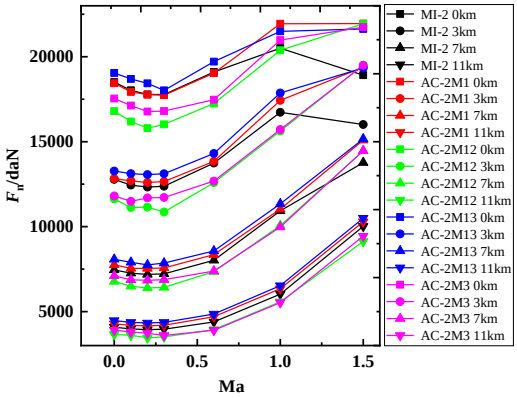

b) AC-2

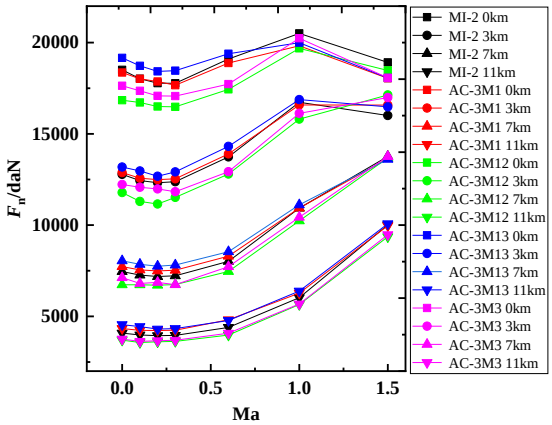

c) AC-3

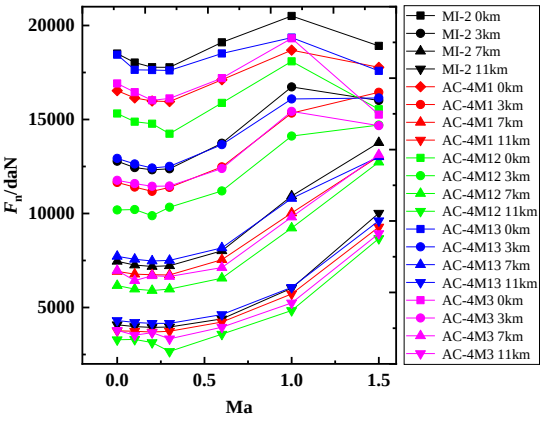

d) AC-4

Fig. 3. Optimization results of speed-height characteristics for different engine configurations

increasing B_1 and B_2, and The F_n increases slightly with the increasing B_3 and B_2 according to Fig. 3 a), b), and c).

Taking the take-off status of the AC-2 adaptive cycle engine as an example, the inlet mass flow and specific thrust for different bypass modes of the adaptive cycle engine are shown in Fig. 4. The m_2 decreases, and F_s increases when the third bypass is closed, and the F_n decreases.

to ensure the lowest fuel consumption with the throttling process.

The *sfc* of the mixed flow turbofan engine is lower than that of the ACE in the initial stage of the throttling line, and the *sfc* mixed flow turbofan engine is higher than that of the ACE in the medium stage of the throttling line. The *sfc* of ACE is reduced after optimization compared to the mixed flow turbofan engine with the

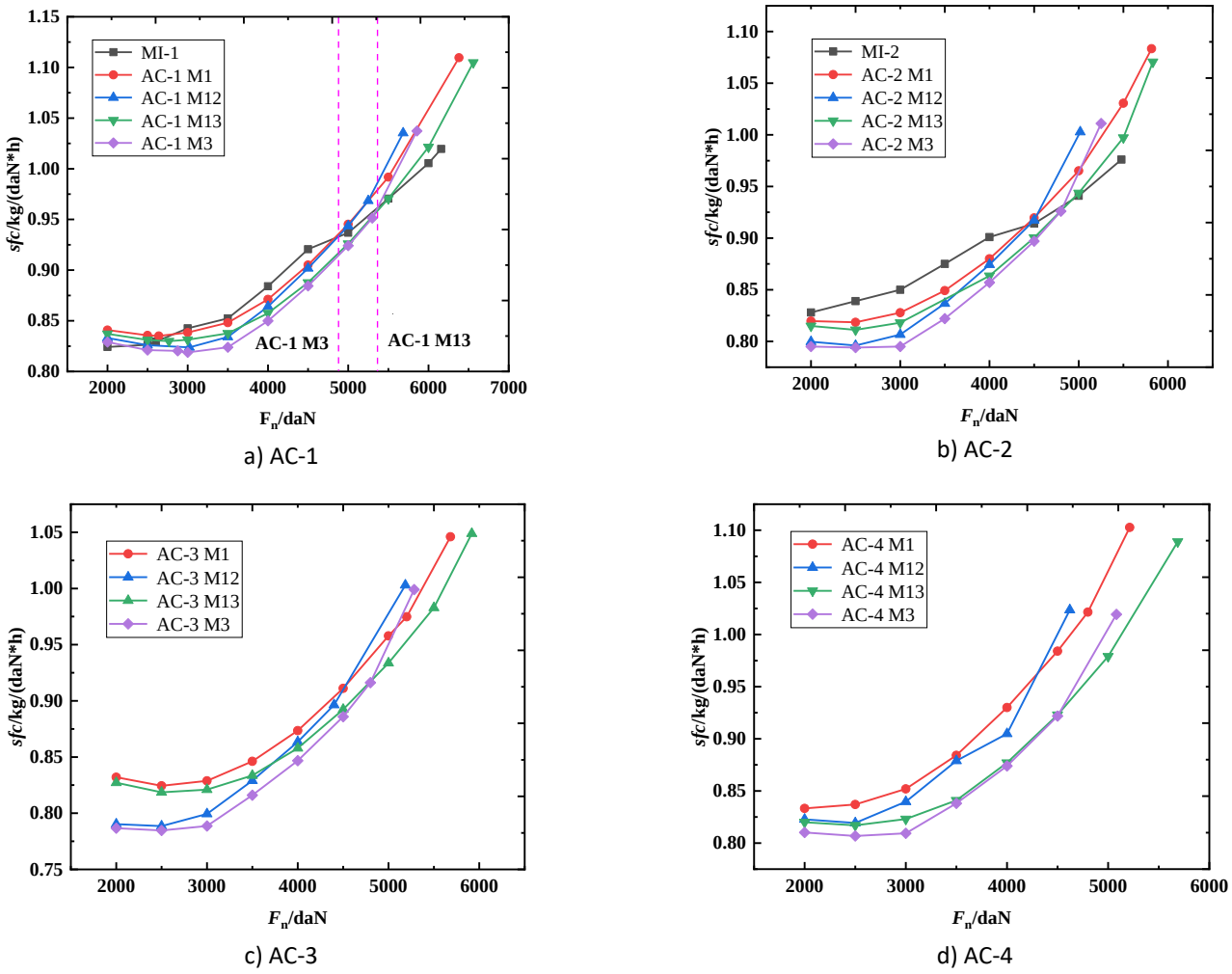

Fig. 5. Optimization results of throttling characteristics for different bypass modes under subsonic conditions

4.2 *Throttling characteristics in subsonic cruis*

The ACE's optimal throttling characteristics for different bypass modes are shown in the Fig. 5 under the subsonic cruise flight conditions (H = 11 km and Ma0 = 0.9). Two optimization strategies are adopted for each optimal throttling characteristics line. For the maximum thrust point in the throttling line, the maximum thrust (Eq. 9) is adopted as the optimization goal. For the other points in the throttling line, the lowest specific fuel consumption (Eq. 10) is adopted as the optimization goal

same B_t, and the optimization ability of the ACE increases with the increase of the B_t. The line distance between mode M1 and M12 increases with the increasing of the B_1 and B_2, and the lines distance between mode M1 and M13 increases with the increase of the B_3.

The optimization results of efficiencies are shown in Fig. 6. As the thrust requirement decreases, the propulsive and thermal efficiencies increase and decrease, respectively. The propulsive efficiency is low,

and thermal efficiency is high when the thrust requirement of the engine is high.

The ACE's optimal throttling characteristics for different engine configurations are shown in the Fig. 7 under the subsonic cruise flight conditions. As the design overall bypass ratio increases, the optimized *sfc* of the ACE decreases. Under the same design overall bypass ratio, the order of advantages in increasing the split ratio is: $B_2 > B_1 > B_3$.

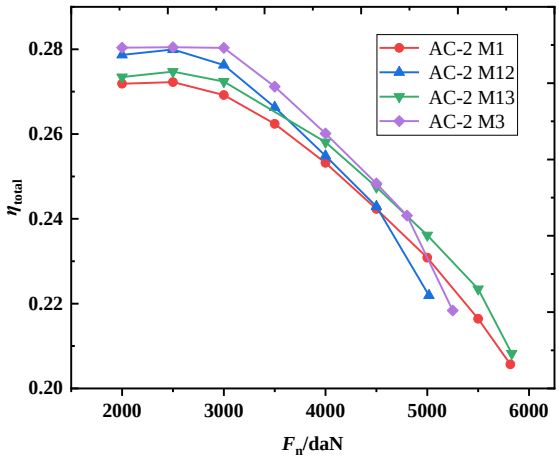

a) Overall efficiency

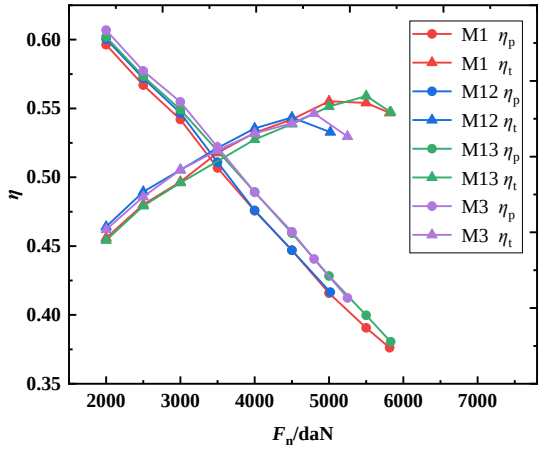

b) Propulsive and thermal efficiencies

Fig. 6. Efficiencies change for different bypass modes under subsonic conditions

4.3 Throttling characteristics in supersonic cruise

The ACE's optimal throttling characteristics are shown in the Fig. 8 under the supersonic cruise flight conditions (H = 15 km and Ma0 = 1.6). Similar to the subsonic cruise state, the sfc of the mixed flow turbofan engine is lower than that of the ACE in the initial stage of the throttling line, and the sfc mixed flow turbofan engine is higher than that of the ACE in the medium stage

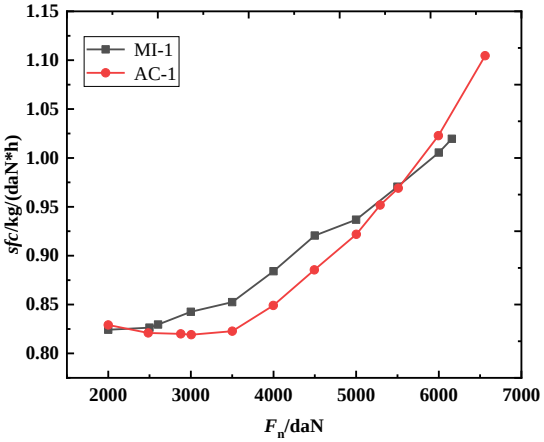

a) Low overall bypass ratio

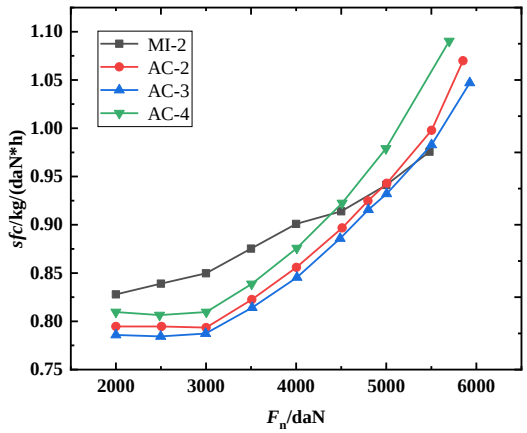

b) High overall bypass ratio

Fig. 7. Efficiencies change for different engine configurations under subsonic conditions

of the throttling line. The modes M13 and M3 have lower sfc than the modes M1 and M12. As the throttling progresses, the modes M1 and M12 with the Flade closed have lower sfc at low thrust requirements.

The optimization results of efficiencies are shown in Fig. 9. As the thrust requirement decreases, the propulsive efficiency increases and the propulsive efficiency of the modes M1 and M12 is the largest. The available pressure ratio of Flade decreases with the decrease of the F_n.

In the initial throttling stages, the mode M13 is more fuel-efficient because of the higher thermal efficiency. In the middle and end throttling throttling stages, the propulsive efficiency of the engine increases. The mode M12 is more fuel-efficient than other modes because of the higher propulsive efficiency.

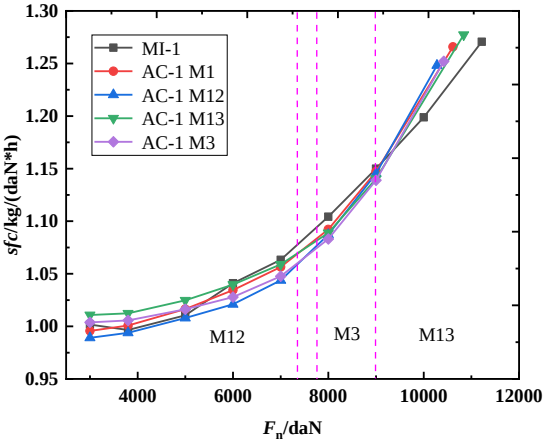

a) AC-1

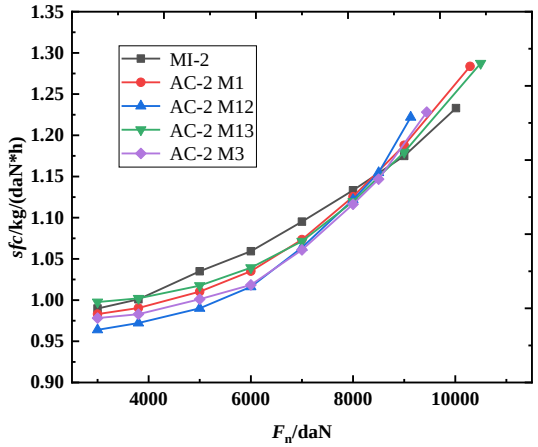

b) AC-2

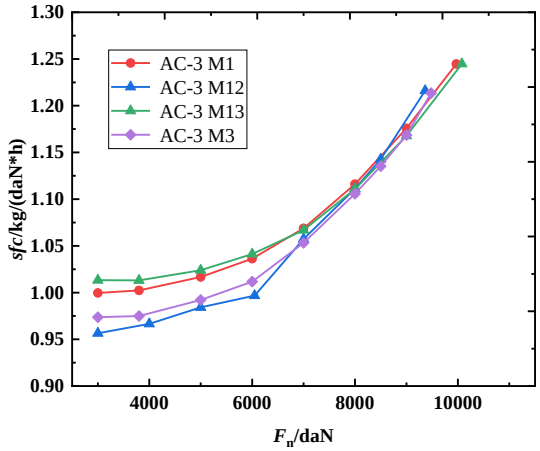

c) AC-3

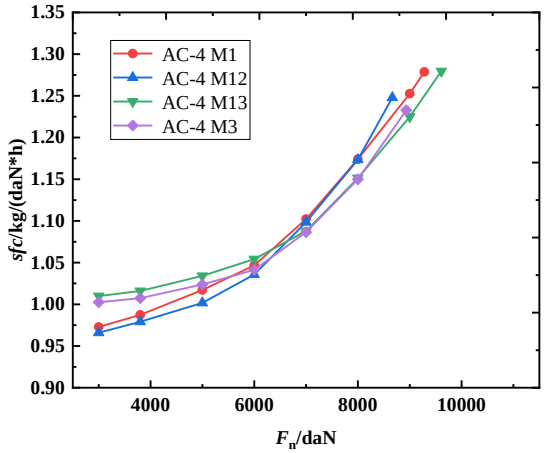

d) AC-4

Fig. 8. Optimization results of throttling characteristics for different engine configurations under supersonic conditions

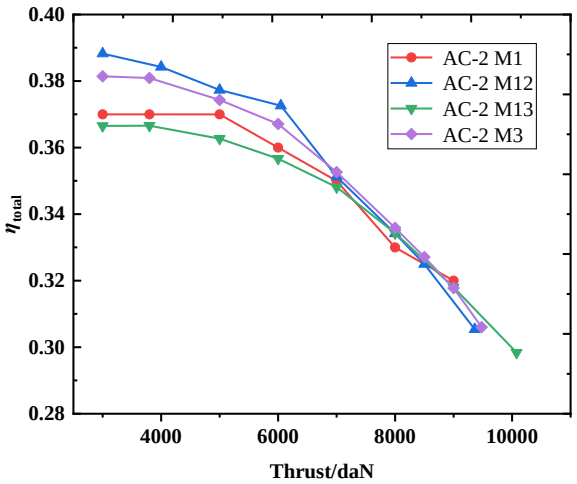

a) Overall efficiency

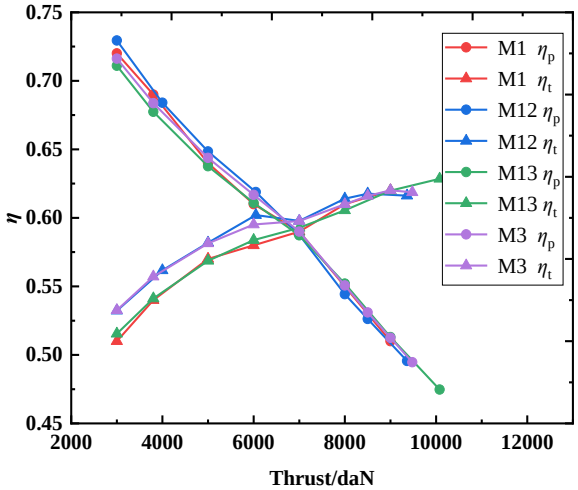

b) Propulsive and thermal efficiencies

Fig. 9. Efficiencies change for different engine configurations under supersonic conditions

The ACE's optimal throttling characteristics for different engine configurations are shown in the Fig. 10 under the supersonic cruise flight conditions. Similar to the subsonic cruise throttling process, as the design overall bypass ratio increases, the optimized *sfc* of the ACE decreases. Under the same design overall bypass ratio, the order of advantages in increasing the split ratio is: $B_2 > B_1 > B_3$.

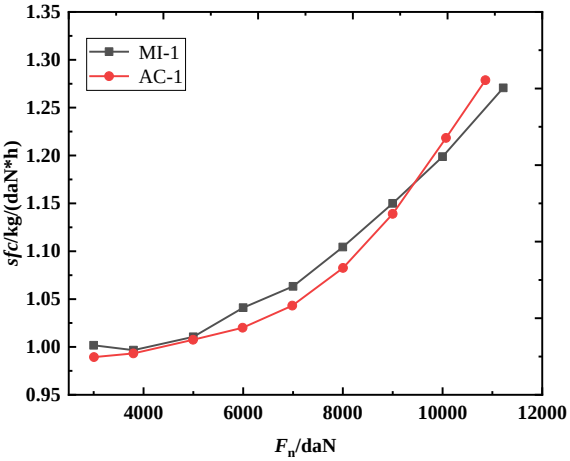

a) Low overall bypass ratio

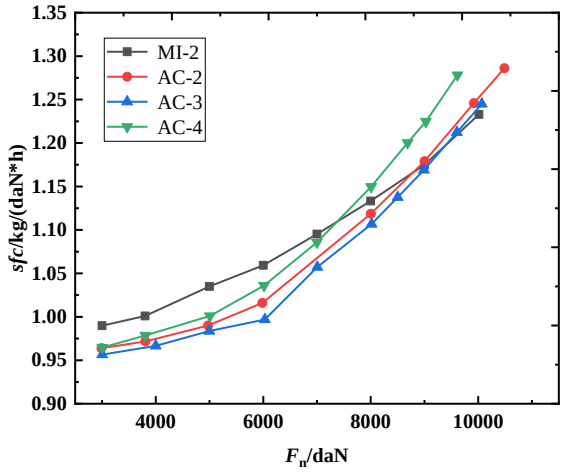

b) High overall bypass ratio

Fig. 10. Efficiencies change for different engine configurations under supersonic conditions

5. CONCLUSIONS

In this study, the performance optimization calculation of the ACE is established based on the PSO, and the impact of the split ratios on the ACE's performance is analyzed. The main conclusions are drawn as follows:

(1) From the speed-height characteristics lines of the ACE with different split ratios, the intermediate thrust increases with the increasing of the B_1 and B_2 under the same B_t. The order of maximum thrust in different working modes is: M13 > M1 > M3 > M12.

(2) Mode switching mode conversion is required to ensure the ACE obtains a wider throttling range and a lower fuel consumption rate. The ACE should work in mode M13 in the initial throttling stages, and mode M3 should be adopted in the middle and end throttling stages. From the subsonic optimal throttling lines, the order of advantages in increasing the split ratio is: $B_2 > B_1 > B_3$.

(3) In the supersonic throttling process, the ACE should work in mode M13 at the initial throttling stages. Modes M3 and M12 should be adopted in the middle and end of the throttle, respectively. From the supersonic optimal throttling lines, the order of advantages in increasing the split ratio is: $B_2 > B_1 > B_3$.

REFERENCE

[1] Aygun H, Cilgin ME, Ekmekci I, Turan O. Energy and performance optimization of an adaptive cycle engine for next generation combat aircraft. Energy 2020; 209:118261.

[2] Buettner R, Roberts RA, Wolff M, Behbahani A. Design of a transient variable cycle turbine engine model for system integration with controls. AIAA Modeling and Simulation Technologies Conference. 2017; AIAA-2017-1940.

[3] Zhang J, Tang H, Chen M. Robust design of an adaptive cycle engine performance under component performance uncertainty. Aerosp Sci Technol 2021; 113(1):106704.

[4] Xu Y, Tang H, Chen M. Design method of optimal control schedule for the adaptive cycle engine steady-state performance. Chin J Aeronaut 2022; 35(4):148-64.

[5] Meng X, Zhu Z, Chen M. Performance Optimization of Adaptive Cycle Engine during Subsonic Climb. Energy Procedia 2019; 158:1613-9.

[6] Zhang J, Dong P, Tang H, Zheng J, Wang J, Chen M. General Design Method of Control Law for Adaptive Cycle Engine Mode Transition. AIAA Journal 2022; 60(1):330-44.

[7] Chen H, Zheng Q, Gao Y, Zhang H. Performance seeking control of minimum infrared characteristic on double bypass variable cycle engine. Aerosp Sci Technol 2021; 108:106359.

[8] Zheng J, Tang H, Chen M. Optimal matching control schedule research on an energy system. Energy Procedia 2019; 158:1685-93.

[9] Wu T, Wu D, Gao S, Song Y, Ren Y, Mou J. Multi-objective optimization and loss analysis of multistage centrifugal pumps. Energy 2023; 284:128638.
[10] Toopshekan A, Abedian A, Azizi A, Ahmadi E, Vaziri Rad MA. Optimization of a CHP system using a forecasting dispatch and teaching-learning-based optimization algorithm. Energy 2023:128671.
[11] Hao W, Wang Z, Zhang X, Zhou L. Acceleration technique for global optimization of a variable cycle engine. Aerosp Sci Technol 2022; 129:107792.
[12] Qian Y, Ye Z, Xu Y, Zhang H. Control performance optimization of variable cycle aero-engine based on MTLBO. Journal of Physics: Conference Series 2020; 1487:012047.
[13] Zhang X, Wang Z. Optimization of FLADE Variable Cycle Engine Performance Based on Improved Differential Evolution Algorithm. Proceedings of ASME 2017 Gas Turbine India Conference. ASME 2017; V001T03A13.
[14] Zheng J, Chen M, Tang H. Matching mechanism analysis on an adaptive cycle engine. Chin J Aeronaut 2017; 30(2):706-18.
[15] Zheng J, Tang H, Chen M, Yin F. Equilibrium running principle analysis on an adaptive cycle engine. Appl Therm Eng 2018; 132:393-409.
[16] Wang T, Yin Z, Tan C, Tian Y, Gao Q, Zhang H. High-power mode control for triaxial gas turbines with variable power turbine guide vanes. Aerosp Sci Technol 2019; 86:132-42.
[17] Chen M, Zhang J, Tang H. Interval analysis of the standard of adaptive cycle engine component performance deviation. Aerosp Sci Technol 2018; 81:179-91.
[18] Sheng H, Chen Q, Li J, et al. Research on dynamic modeling and performance analysis of helicopter turboshaft engine's start-up process. Aerosp Sci Technol 2020; 106:106097.
[19] Hanachi H, Liu J, Mechefske C. Multi-mode diagnosis of a gas turbine engine using an adaptive neuro-fuzzy system. Chin J Aeronaut 2018; 31(1):1-9.
[20] Zhou Q, Yin Z, Zhang H, Wang T, Sun W, Tan C. Performance analysis and optimized control strategy for a three-shaft, recuperated gas turbine with power turbine variable area nozzle. Appl Therm Eng 2020; 164:114353.
[21] Kennedy J, Eberhart R. Particle swarm optimization. Proceedings of ICNN'95 - International Conference on Neural Networks. IEEE 1995; 5263228.
[22] Zhao R, Zhang H, Song S, Yang F, Hou X, Yang Y. Global optimization of the diesel engine–organic Rankine cycle combined system based on particle swarm optimizer. Energy Conversion and Management 2018; 174:248-59.
[23] Lavanya R, Murukesh C, Shanker NR. Microclimatic HVAC system for nano painted rooms using PSO based occupancy regression controller. Energy 2023; 278:127828.